Evaluation of aerodynamic drag of a full-scale cyclist model by large-scale tomographic-PIV

Terra, Wouter; Sciacchitano, Andrea; Scarano, Fulvio

Publication date
2016

Document Version
Accepted author manuscript

Published in
Proceedings of the International Workshop on Non-Intrusive Optical Flow Diagnostic

International Workshop on Non-Intrusive Optical Flow Diagnostics
Delft | The Netherlands • October 25 – 26, 2016

Evaluation of aerodynamic drag of a full-scale cyclist model by large-scale tomographic-PIV

W. Terra[1,*], A. Sciacchitano[1], F. Scarano[1]
1: Aerospace Engineering Department, TU Delft, The Netherlands
* Correspondent author: w.terra@tudelft.nl

Keywords: Tomographic PIV, aerodynamic drag, HFSB, large-scale measurements, cycling aerodynamics

ABSTRACT

Experiments are conducted to determine the drag of a full-scale cyclist model in a wind tunnel at 4 m/s. The aerodynamic drag is evaluated from tomo-PIV measurements in the wake of the model applying the conservation of momentum within a control volume. The measurements are conducted in a thin volume of 100 x 170 x 3 cubic centimeters using helium-filled soap bubbles as flow tracers. The aerodynamic drag from PIV measurements is compared to standard balance measurements, obtaining an agreement between the two results within 2%.

Introduction

The aerodynamic drag acting on a cyclist on a flat road is the main resistive force the athlete has to overcome. Kyle and Burke (1984) report a contribution of 90% at 8.9 m/s, while other find values up to 96% at 14 m/s (Gibertini and Grassi, 2008, Martin et al., 1998). Drag reductions of one percent can result in time savings of 15 seconds in a 50 km time-trial (Spurklund et al. 2015). Considering that the difference between the winner and runner up in the UCI World Championships in the men's individual team time-trial was 5 seconds over a course of 46.2 km, these drag reductions clearly have a major impact.

Most authors have investigated the effect of changes in posture, garment and equipment, directly measuring the aerodynamic forces acting on the model by a balance system (Zdravkovich 1996, for example). This approach, however, is blind to the flow structures around the athlete responsible for the generation of the aerodynamic forces, and is, therefore limited in terms of future drag minimization (Lukes et al. 2005). Recently, first steps have been taken to characterize the flow over a cyclist and relate the changes in the large flow structures with variations in aerodynamic drag (Crouch et al. 2013; Barry et al. 2016), providing a better understanding of cycling aerodynamics. Also in these works the aerodynamic forces acting on the bike-rider system were measured by a force balance.

Instead, the aerodynamic drag acting on a model can be derived from quantitative flow visualizations using the conservation of momentum (e.g. van Oudheusden et al. 2007, Kurtulus et al. 2007), allowing to relate changes in model geometry and orientation, to variations in the flow structures and forces acting on the model, from velocity information only. The application of this approach to bluff bodies exhibiting a complex three-dimensional flow, has been limited to objects sizes in the order of centimeters (Ragni et al. 2012, Terra et al. 2016). A demonstration of the approach on the human-scale is missing.

This work proposes for the first time to measure the aerodynamic drag of a full-scale cyclist from PIV data. Tomographic PIV measurements are conducted to obtain the velocity in a thin wake volume behind a mannequin. The computed aerodynamic drag is compared to balance data to assess the accuracy of the method. Finally, this work can be considered as a mile-stone towards the on-site application of this technique to measure the drag of moving cyclists outside of a wind tunnel.

Methodology

In an unconfined flow the time-averaged drag of an object can be derived from velocity data in a wake plane only, provided that this plane is located sufficiently far downstream of the object (Ragni et al. 2012; Terra et al, 2016):

$$\bar{D} = \rho \iint_{S_{wake}} (U_\infty - \bar{u})\bar{u}\, dS - \rho \iint_{S_{wake}} \overline{u'^2}\, dS + \iint_{S_{wake}} (p_\infty - \bar{p})\, dS \quad (1)$$

where $\bar{u}$ is the time-average streamwise velocity, u' the fluctuating streamwise velocity and $\bar{p}$ the time-average pressure in the wake plane S. U_∞ and p_∞ are the freestream velocity and pressure, respectively, and ρ the flow density, which is constant in an incompressible flow. The time-average pressure is evaluated from velocity statistics solving the Poisson equation for pressure, according to van Oudheusden (2013). When assuming irrational flow, the pressure integral in Equation (1) can be replaced by an induced drag term containing the in-plane velocity components (Noca et al. 1999):

$$\bar{D} = \rho \iint_{S_{bc}} (U_\infty - \bar{u})\bar{u}\, dS\rho - \rho \iint_{S_{bc}} \overline{u'^2}\, dS + \frac{1}{2}\rho \iint_{S_{bc}} (\bar{v}^2 + \bar{w}^2 + \overline{v'^2} + \overline{w'^2})\, dS \quad (2)$$

Although the flow behind the model is not irrational, the approach has been successfully used to estimate drag variations in cycling (Crouch et al. 2013) and is, therefore, considered here as well as an alternative that does not require the reconstruction of pressure.

Experimental apparatus and procedure

The experiments are conducted in the Open Jet Facility wind tunnel in the Aerodynamic Laboratories of Delft University of Technology Delft. The octogonal cross-section of the wind tunnel produces a jet of 2.85 m x 2.85 m with a maximum of 0.5% turbulent intensity. A mannequin was manufactured thermoplastic polyester by 3D-printing after scanning a professional cyclist in time-trial position. The mannequin is installed on a Giant Trinity Advanced Pro frame (2017 model) equipped with a Shimano Dura Ace 9070 group set, Shimano 9000 C75 front wheel and a Pro Texreme Wide disc wheel with Vittoria Corsa 25mm tubulars (Fig. 1-right). The position of the rider's legs is fixed at 75° crank angle. Table 1 contains further details of the size and position of the model. The front and rear axis of the bike are fixed onto a 6-component balance that is shielded from the outer flow by a ground plate.

Three Fast CAM SA1 cameras (CMOS, resolution of 1024 x 1024 pixels, pixel pitch of 20 µm, 12 bit) image an area of about 3.5 m^2, located one meter behind the mannequin's lower back, resuting in a magnification factor of about 0.01. Two cameras are equipped with a 35 mm Nikkor lens and one with a 50 mm one, all set to f/5.6, and illumination is provided by a Nd:YAG continuum Mesa PIV laser from the side of the test section. A sketch of the experimental setup is reported in Fig. 1-left.

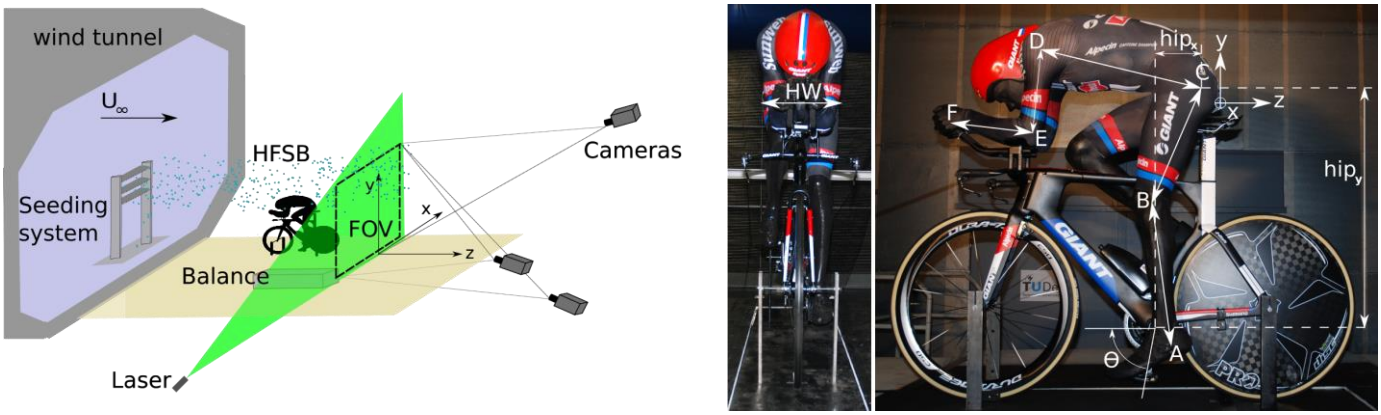

Fig. 1: Illustration of the experimental setup (left); Mannequin position and dimensions (right)

Helium-filled soap bubbles (HFSB) are used as flow tracers. The bubbles are injected into the flow by three aerodynamic rakes located at the exit of the wind tunnel (Fig. 1-left). The air, helium and soap fluid flow rates are controlled by a fluid supply unit provided by LaVision GmbH. The three rakes seed an area of about 700 x 700 mm^2 along x and y. The rakes are translated along x and y (4 different height locations and 4 different spanwise locations, for a total of 16 different locations) to seed the entire measurement domain with flow tracers. For each rake position, a total of 272 double-frame image pairs are collected at

200 Hz in Davis 8.3 at a velocity of 4 m/s. Velocity fields are reconstructed in thin volumes of about 700 x 700 x 30 mm^3 in x-, y- and z-direction with a density of 0.75 vectors/cm. The vector fields consist of three planes in volume depth, which allows to compute the out of-plane velocity gradients in the middle plane. Finally, the overlapping regions of the 16 individual velocity fields are integrated and small empty regions are filled by interpolation to obtain the velocity statistics in a volume of 1000 x 1700 x 30 mm^3 in the wake of the cyclist (Fig. 1-left). Additionally, 25 balance measurements are conducted at different rake positions to compare to the drag derived from the PIV data.

Table 1: Mannequin position and size characteristics

Name	Symbol	Angle/distance	Name	Symbol	distance
Crank angle	θ	75	Lower leg	A-B	475 mm
Hip width	HW	365 mm	Upper leg	B-C	460 mm
Shoulder width	SW	380 mm	Torso	C-D	600 mm
Hip location (x)	Hip_x	180 mm	Upper arm	D-E	326 mm
Hip location (y)	Hip_y	850 mm	Lower arm	E-F	290 mm

Results

The time-average velocity behind the mannequin corresponds well to the flow topology in the wake of a cyclist described by Crouch et al. (2013) by dynamic pressure probe, even though the Reynolds number of our study is a factor four lower. Streamwise vortex structures, originating from the hips and lower back of the rider, are observed about one meter above the floor (Fig. 2-left and right). Strong streamwise vortices are also present in the wake of the lower leg and feet of the model. Furthermore, an area of low streamwise velocity is located behind the hip of the stretched leg (Fig. 2-right) and another area of low velocity is present behind the rear wheel's axis, which are the main contributors to the aerodynamic drag. The described vortex structures also contribute to the aerodynamic drag through the induced drag term in Equation (2).

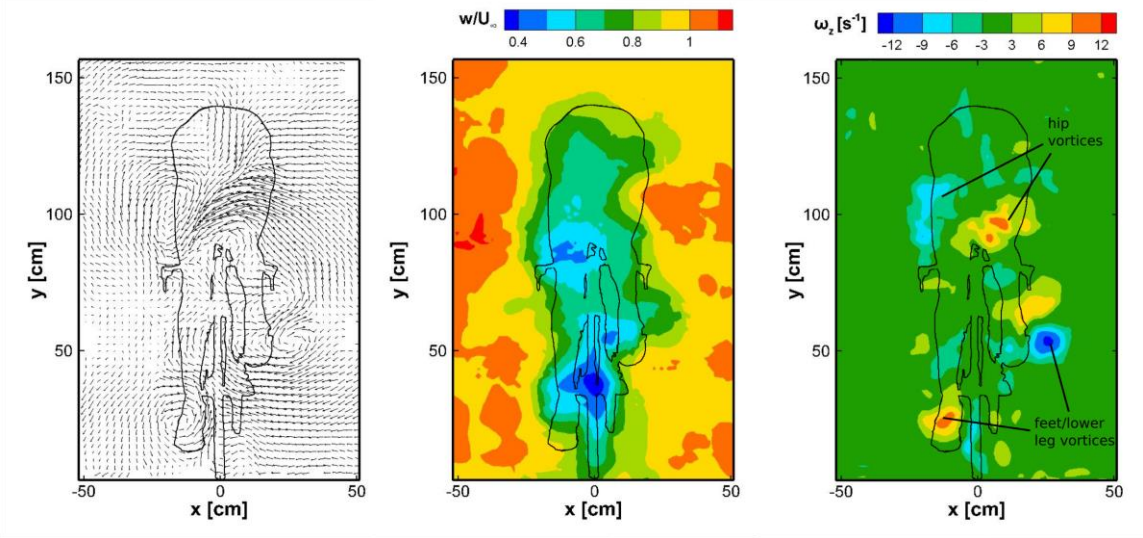

Fig. 2: Velocity in the wake of the mannequin; vector field (left), non-dimensional streamwise velocity (middle) and streamwise vorticity (right).

To evaluate the contribution of Reynolds stress and time-average pressure to the aerodynamic drag, Fig. 3 presents the contours of the two quantities. A region with high velocity fluctuations corresponds to the location of the left upper-hip vortex (Fig. 2-right). This may be explained by the fact that the open hip orientation (stretched left leg) produces a coherent shear layer, whose oscillations cause large velocity fluctuations. Instead, on the right side of the mannequin the hip angle is closed and the knee is oriented upstream, yielding smaller-scale velocity fluctuations. The asymmetry in the Reynolds stress field is

also observed in the spatial distribution of the pressure coefficient. The low pressure area at the right corresponds to a relatively high streamwise velocity area (Fig. 2-middle) and high streamwise vorticity region (Fig. 2-left). This combination may explain the low pressure at this side of the mannequin.

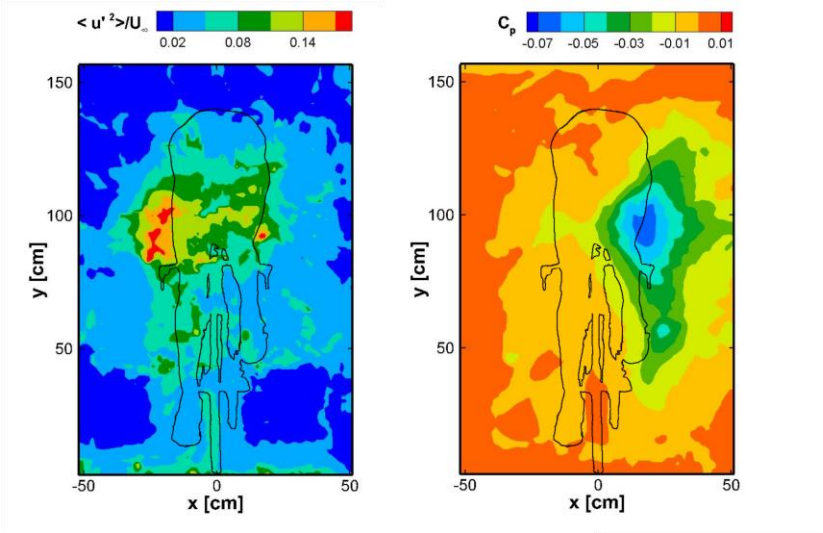

Fig. 3: Contours of the normal Reynolds stress (left) and the time-average pressure coefficient (right).

The resulting aerodynamic drag computed by the control volume approach are presented in Table 2. The assumption of irrotational flow results in an underestimation of the drag by about 2%. Although the two values are close, exactly such differences need to be measurable in order to evaluate drag reductions due to change of posture or surface roughness. Therefore, for an accurate drag estimate the pressure term needs to be considered and not replaced by the induced drag term. Comparison with force balance measurements shows that both drag results from PIV are within one standard deviation of the former. Therefore, both methods seem to be sufficiently accurate to obtain the drag of the full-scale cyclist at 4 m/s within the accuracy range of the balance system.

Table 2: Aerodynamic drag of the mannequin at 4 m/s computed by the control volume methodology, including the different terms contributing to the drag, and measured by the force balance.

Method	**Drag [N]**	**Momentum term**	**Pressure term**	**Reynolds stress term**	**Induced drag term**
Control volume approach	2.39	2.60	0.11	-0.32	-
Control volume approach (irrotational flow assumption)	2.34	2.60	-	-0.32	0.07
Force balance	2.38 (sd = 0.04)	-	-	-	-

Conclusions

The drag of a cyclist mannequin is derived from velocity statistics in the wake of the model, obtained with large scale tomo-PIV using HFSB as flow tracers, applying a control volume approach. It is the first time this approach is demonstrated at the human scale. The measured velocity field compares well to the flow topology described in literature, showing complex streamwise vortex structures originating from different parts of the cyclist. The drag of the mannequin is also measured by a force balance to assess the accuracy of the control volume approach. It is concluded that, in the present conditions, the control volume approach allows to measure the drag within the accuracy range of standard balance measurements.

Acknowledgements

This work is partly funded by the TU Delft Sports Engineering Institute and the European Research Council Proof of Concept Grant "Flow Visualization Based Pressure" (no. 665477). Martyna Goral and Laurens Voet are kindly acknowledged for the support on the experiments.

References

1. Barry N, Burton D, Sheridan J, Thompson M, Brown NAT (2016) An analysis of the wake of pedalling cyclists in a tandem formation, 11th conference of the International Sports Engineering Association, Procedia Engineering 147, 7-12, ISEA 2016
2. Crouch TN, Burton D, Brown NAT, Thomson MC, Sheridan J. (2014) Flow topology in the wake of a cyclist and its effect on aerodynamic drag, J Fluid Mech, vol 748, 5-35
3. Gibertini G and Grassi D (2008) Cycling Aerodynamics, in Sport Aerodynamics, Helge Nørstrud Editor 20
4. Grappe F, Candau R, Belli A, Rouillon JD (1997) Aerodynamic drag in field cycling with special reference to Obree's position, Ergonomics, vol 40, no 12, 1299 – 1311
5. Kurtulus DF, Scarano F, David L (2007), Unsteady aerodynamic forces estimation on a square cylinder by TR-PIV, Exp Fluids, 42:185-196
6. Kyle CR and Burke ER (1984) Improving the racing bicycle, Mech Engng 106 (9), 34–45
7. Lukes RA, Chin SB, Haake SJ (2005) The understanding and development of cycling aerodynamics, Sports Engineering 8, 59-74
8. Noca F, Shiels D, Jeon D (1999) A comparison of methods for evaluating time-dependent fluid dynamic forces on bodies, using only velocity fields and their derivatives. J Fluid Struct, 13:551–578
9. Martin et al. (1998) Validation of a mathematical model for road cycling power, J Appl Biomech 14, 276–291
10. Ragni D, van Oudheusden BW, Scarano F (2012) 3D pressure imaging of an aircraft propeller blade-tip flow by phase-locked stereoscopic PIV, Exp Fluids, 52:463-477
11. Spurklund L, Bardal LM, Seatran L, Oggiano L (2015) Low Aerodynamic Drag Suit for Cycling - Design and Testing, Proceedings of the 3rd International Congress on Sport Sciences Research and Technology Support, 89-96, Lisbon, Portugal
12. Terra W, Sciacchitano A, Fulvio S (2016) Aerodynamic drag of transiting objects by large-scale tomographic-PIV, Proceedings 18th International Symposium on applications of laser and imaging techniques to fluid dynamics, 1135-1153
13. van Oudheusden et al. (2007) Evaluation of integral forces and pressure fields from planar velocimetry data for incompressible and compressible flows, Exp Fluids 43:153-162
14. van Oudheusden BW (2013) PIV-based pressure measurement, Meas Sci Technol. 24 032001 (32pp)
15. Zdravkovich MM, Ashcroft MW, Chisholm SJ, Hicks N (1996) Effect of cyclist's posture and vicinity of another cyclist on aerodynamic drag, The Engineering of Sport 1, 21-28